RSC Advances

PAPER

View Article Online
View Journal | View Issue

Cite this: *RSC Adv.*, 2024, **14**, 30091

Efficient synergism of concentric ring structures and carbon dots for enhanced methanol electro-oxidation†

Cong Xiang,‡[a] Yunyun Ling,‡[a] Zitong Zhou,[a] Xiaoyu Zhu,[a] Fan Xue,[a] Zhijun Feng,[a] Yiwei Wang,[a] Xinyi Cheng,[a] Meifang Wang *[a] and Xiaomei Cheng*[ab]

Developing affordable and reliable electrocatalysts with high activity and stability is crucial for enhancing the practicality of direct methanol fuel cells (DMFCs). An effective and simple strategy of combining the carbon point of N-CDs (0.4 mg mL^{-1}) with NiO/Ni for the fabrication of NiO/Ni–N-CDsV nanocomposites with a three-dimensional concentric core–shell structure was proposed to successfully prepare the electro-oxidation catalyst of methanol. The low cost of Ni-based materials and the conductive N-CDs that improve methanol catalytic performance make the composites an excellent choice as electrode materials for direct methanol fuel cells (DMFCs). The electrocatalytic behavior of methanol oxidation was studied using cyclic voltammetry and chronoamperometry. The results indicated that the catalytic activity of NiO/Ni–N-CDsV increased by 3.02 times, and the current density was stable during the operation for 83 hours, implying strong electrocatalytic stability. Furthermore, the electrocatalytic performance for ethanol, ethylene glycol, and glycerol electro-oxidation reactions was impressive. This study provides a novel foundation for the development of high-performance, cost-effective, non-noble metal catalysts for DMFC applications, contributing to the formation of commercially competitive electro-oxidation catalysts with enhanced efficiency and stability.

Received 27th June 2024
Accepted 31st August 2024

DOI: 10.1039/d4ra04685d

rsc.li/rsc-advances

1. Introduction

Direct methanol fuel cells (DMFCs) have attracted considerable attention for application in electric vehicles, drones, and portable electronic devices, owing to their eco-friendliness, affordability, easy transport, and high energy efficiency.[1–4] However, the commercialization of DMFCs is primarily dependent on the kinetics of the anodic methanol oxidation reaction (MOR),[5] which has traditionally relied on the use of noble metal platinum (Pt) as an anode catalyst material owing to its high activity.[6–9] Pt-X alloys are used, X refers to metals such as PtCu,[10,11] PtRu,[12,13] and PtCo[14] or design different nanostructures such as nanorods, nanosheets, nanoblocks.[15] Although the importance of different aspects of auxiliary catalysts or morphological tuning in fuel cell catalyst design and fabrication has been revealed, the high cost of Pt and the inhibitory effects of carbonaceous intermediates, such as CO, significantly impede the widespread application of Pt catalysts.[16–20] Therefore, there is an urgent need to develop non-Pt nanocatalysts that exhibit high electrocatalytic performance for the MOR.

Transition metals such as copper (Cu), cobalt (Co), nickel (Ni), and iron (Fe), along with their compounds, have been extensively explored as alternative fuel cell catalysts owing to their abundance, cost-effectiveness, and favorable electrical conductivity.[21–23] Researchers have investigated non-Pt-based catalysts such as metal carbides, transition metal oxides, and non-Pt transition metal alloys for the methanol oxidation reaction (MOR).[24–29] Notably, Pt-free Ni_3B/Ni catalysts have been reported to possess exceptionally high reactivity and an extended lifetime. The stability and selectivity of the methanol oxidation reaction are improved by the ability of methanol to prevent the phase transformation of the electrocatalyst into higher-valent electro-oxidation products.[30] The excellent surface activity and high economic efficiency of nickel-based catalysts hold a broad prospect for application in methanol electro-oxidation reactions.

Carbon materials, which possess good conductivity as well as electrochemical stability, are very important in the MOR. Chen *et al.* prepared tubular $NiCo_2S_4$/carbon nanotube (CNT) nanocomposites by combining conductive carbon nanotubes with tubular $NiCo_2S_4$. The results showed that the incorporation of CNTs further improved the performance of the DMFC.[31] The use of carbon nanotubes also lays the foundation for later studies of

[a]*Department of Pharmacy, Wannan Medical College, Wuhu 241002, China. E-mail: zijingyuwinter@163.com; chengxm@wnmc.edu.cn*

[b]*State Key Laboratory of Coordination Chemistry, Nanjing University, Nanjing 210023, China*

† Electronic supplementary information (ESI) available. See DOI: https://doi.org/10.1039/d4ra04685d

‡ These authors contributed equally to this work.

related carbon materials in fuel cell systems. Carbon quantum dots, as a new type of nanomaterial in the carbon family, have been widely used in many fields such as medical imaging technology, environmental monitoring, chemical analysis, catalyst preparation, and energy development in recent years owing to their advantages of good water solubility, low toxicity, environmental friendliness, wide source of raw materials, low cost, and good biocompatibility.[32–34] The doping of carbon dots with heteroatoms such as nitrogen, phosphorus, and sulfur leads to an increase in the quantum yield, which enriches the electronic properties of carbon dots. Nitrogen-doped carbon dots (N-CDs) have attracted much attention owing to their excellent conductivity and charge transport capacity.[35] Wu *et al.* prepared a series of NCQDs and investigated the correlation between the nitrogen content and their electrocatalytic performance.[36]

Previous studies have shown that noble metal-containing catalysts are mostly used in combination with carbon materials, and non-precious metal materials are rarely used in combination with carbon dots. Therefore, in this study, we used a non-precious metal nickel-based catalyst NiO/Ni and N-CDs to synthesize three-dimensional, concentric ring core–shell nanostructures with an opening shell surface of NiO/Ni–N-CDsV. A series of NiO/Ni–N-CDsV composites containing three-dimensional concentric ring core–shell nanostructures with different concentrations of carbon dots were prepared, and the performance for electrocatalytic methanol electrooxidation was optimized. The incorporation of N-CDs resulted in an improved electrocatalytic activity for methanol oxidation compared to the pristine catalyst. Notably, the electrocatalytic performance does not exhibit a strictly positive correlation with the concentration of N-CDs. However, the addition of just 0.05 mL of N-CDs resulted in a peak current density of 47.32 mA cm^{-2}, a 3.02 times improvement from the original catalyst. The surface of N-CDs is rich in oxygen-containing functional groups, which are beneficial for enhancing conductivity, reducing electrochemical impedance, facilitating electron transfer, and augmenting redox activity. In addition, the distinctive concentric ring structure provides both accessible interior and exterior surfaces, as well as a high number of exposed active sites, which collectively contribute to the enhanced electrocatalytic activity.

2. Experimental section

2.1 Chemicals

Sodium hypophosphite (NaH_2PO_2), *N*,*N*-dimethyl formamide (DMF), potassium hydroxide (KOH), sodium hydroxide (NaOH), nickel chloride hexahydrate, analytical grade methanol, ethanol, ethylene glycol and glycerol were provided by Sinopharm Chemical Reagent Co., Ltd (Shanghai, China). Sodium lauryl sulfate (SDS) was purchased from Fuchen Chemical Reagent Co., Ltd. Carbon black was purchased from Jiuding Chemical. Nafion solution was supplied by Suzhou Shengnuo Technology Co., Ltd. All reagents and chemicals were analytically pure.

2.2 Preparation and purification of nitrogen-doped carbon dots

First, 0.2619 g (2.4 mmol) of *m*-aminophenol (*m*-AP) was weighed and dissolved in 50 mL of ultrapure water using a vortex mixer, the pH value of the solution was adjusted to 2.5 with dilute nitric acid, and dissolved oxygen was removed by passing nitrogen or argon gas into the solution for 30 min. Next, the solution was dispensed into three 25 mL Teflon-lined stainless-steel autoclaves and again vented with nitrogen or argon for 5–10 min, respectively. Finally, it was heated in a blast dryer at 170 °C for 4 h and removed after cooling naturally to room temperature. The initial product of the hydrothermal synthesis was a dark brown solution. Separation and purification consist of three main components, roughing filter, extraction, and Silica Gel Column Chromatography, and the initial product of the reaction was first passed through a 0.22 μm mixed cellulose filter (aqueous phase) to remove large particles, and then concentrated to about 5 mL using a rotary evaporator (60 °C). Extraction was carried out by adding 5 mL of ethyl acetate (EAC) to obtain a translucent bright yellow aqueous solution. The above solution was then added to a silica gel column (the stationary phase was 300–400 mesh silica gel powder) and the mobile phase was a mixture of EAC and methanol (from 2 : 1 by volume). With the addition of the mobile phase, the blue, anthocyanin, green and yellow fluorescence of the four components flowed out sequentially. Finally, the yellow fluorescence of the carbon dots (0.4 mg mL^{-1}) was obtained.

2.3 Synthesis of Ni nanospheres

SDS (0.1 g), $NaH_2PO_2 \cdot H_2O$ (0.848 g) and $NiCl_2 \cdot 6H_2O$ (0.4754 g) were dispersed into 10 mL deionized water. Then, 5 mL DMF and 5 mL 5.0 M NaOH aqueous solutions were in turn added into the above solution. After that, the mixed solution was transferred into a Teflon-lined stainless-steel autoclave with 25 mL capacity and maintained at 160 °C for 10 h. After the mixture was gradually cooled to room temperature, the black magnetic products were obtained using a magnet, washed several times with deionized water, and dried for 5 h at 60 °C under reduced pressure.

2.4 Synthesis of NiO/Ni

An appropriate amount of Ni nanospheres were taken in a porcelain boat and subjected to air calcination in a tube furnace at 350 °C for 2 h at a rate of 5 °C min^{-1} in air.

2.5 Synthesis of NiO/Ni–N-CDs

First, 0.1 g of NiO/Ni was added to 20 mL ethanol by ultrasonication for 20 min. Then 0.03 mL carbon dots and 0.97 mL ethanol were added to the above solution and sonicated for 30 min. The final mixture was transferred to a 40 mL Teflon autoclave and kept at 120 °C for 4 h. Afterward, the precipitate was abstracted by centrifugation and rinsed thoroughly with ethanol. Then the as-obtained mixture was evaporated to dryness at 60 °C and denoted as NiO/Ni–N-CDs0.03. The

preparation process was the same as that of the NiO/Ni–N-CDs0.03, except that the mixture of 0.03 mL carbon dots and 0.97 mL ethanol was replaced by a mixture of 0.05 mL carbon dots and 0.95 mL ethanol or 0.08 mL carbon dots and 0.92 mL ethanol. The products were denoted as NiO/Ni–N-CDs0.05 and NiO/Ni–N-CDs0.08. Similarly, we replaced NiO/Ni with Ni nanospheres and synthesized samples using the same procedure and named them Ni–N-CDs.

2.6 Characterization methods

X-ray diffraction (XRD) patterns were acquired using a D/tex Ultra-high-speed 1D semiconductor array explorer of X-ray powder diffraction (XRD, MiniFlex600) to study the crystal structures. Scanning electron microscopic (SEM) images were acquired using a Hitachi S-4800 field emission scanning electron microscope at an operating voltage of 5 kV. The morphology and structures of the samples were observed by transmission electron microscopy (FEI Tecnai G2 F20 S-Twin 200 kV). Electronic states and elemental compositions were analyzed by Energy-Dispersive X-ray Analysis (EDX) (B5∼U92). The Brunauer–Emmett–Teller (BET) surface area and pore distribution of the samples were determined by nitrogen adsorption–desorption measurements (Micromeritics ASAP 2460/2020, USA). X-ray photoelectron spectra (XPS, Thermo Fisher Scientific K-Alpha) were recorded using a spectrometer with AlKα radiation (1486.8 eV).

2.7 Electrochemical measurements

Electrocatalyst powder inks were prepared using a mixture of 0.1 mL deionized water, 0.85 mL ethanol, 0.05 mL Nafion solution, 5 mg of the catalysts and 5 mg of carbon black followed by ultrasonication for 30 min. Then 50 μL of ink was uniformly loading on Carbon Paper for use as the working electrode with a catalyst loading of 0.25 mg cm^{-2}. All electrochemical measurements were performed in a conventional three-electrode system using an electrochemical workstation (CHI 660E, Shanghai CH Instruments, Inc.) in a 1 M KOH + 1 M CH_3OH solution. The Carbon Paper with the electrocatalyst ink was used as the working electrode, while a Pt wire and a Ag/AgCl electrode were used as the counter and reference electrodes. The MOR performances of electrocatalysts were recorded using cyclic voltammetry (CV) scans from 0 V to 0.7 V *vs.* Ag/AgCl at a scan rate of 50 mV s^{-1}. The stability test was performed by a chronoamperometry method using 0.6 V *vs.* Ag/AgCl. The activity of ethanol, ethylene glycol, and glycerol oxidation reaction was performed in 1 M KOH coupled with 1 M ethanol, ethylene glycol, and glycerol, respectively.

3. Results and discussion

3.1 Synthesis and characterization of NiO/Ni–N-CDs

In the synthesis process (Scheme 1), spherical Ni was first prepared by a one-step solvothermal method. Subsequently, NiO/Ni was obtained by incomplete calcination in air as the original Ni-based catalyst. The carbon dots were decorated onto the NiO/Ni catalyst by adding different volume solutions of highly purified carbon dots, and the final sample was denoted as NiO/Ni–N-CDsV. The absorption spectra (Fig. S1†) and emission spectra (Fig. S2†) were carried out to demonstrate the successful preparation of N-CDs. By EDS characterization of single CDs, it was found that the N atom content reached 5% (Fig. S3†). The following discussion mainly focused on the sample introduced to 0.05 mL N-CDs (denoted as NiO/Ni–N-CDs0.05). As shown in Fig. S4a,† we recorded the visible absorption spectra of NiO/Ni–N-CDs0.05 in the range of 200–800 nm, and the main absorption peaks were consistent with the pure N-CDs. The bandgap of NiO/Ni–N-CDs0.05 belongs to the direct bandgap (formula (S1)†), and the bandgap value was obtained by plotting a graph through Tauc's relation as 2.19 eV (Fig. S4b†).

To verify that the sample was successfully prepared, the phase composition and the crystal structure were investigated by powder X-ray diffraction (PXRD) patterns of all the as-synthesized samples (Fig. 1a). The main characterization peaks are cubic Ni (PDF #04-0850) and cubic bunsenite NiO (PDF #47-1049), indicating that the Ni was partially oxidized to NiO. The modification of N-CDs did not change the position of the characteristic peaks of the original NiO/Ni catalyst. There is no observable peak from N-CDs due to the limited amount of composite catalysts.[37] We performed scanning electron microscopy (SEM) and transmission electron microscopy (TEM) to examine the morphology and microstructure of the synthesized samples for observing how the samples changed with the experiments. Fig. 1b shows the SEM image of Ni with spherical morphology, and the average size is approximately 110 nm (inset Fig. 1b). The NiO/Ni catalyst retains a spherical shape and the average size has increased slightly (Fig. 1c). The catalyst size is further increased with the introduction of N-CDs (Fig. 1d), and the hollow structures are found in the SEM image inset in Fig. 1d. Meanwhile, with the increase in CD content, the proportion of the hollow structure increases until the NiO/Ni–N-CDs0.08 structure partially collapses (Fig. 1e and f).

More explicit and detailed internal structural features were observed from the TEM and high-resolution TEM (HRTEM) images, which were determined to be consistent with the previous experimental results. NiO/Ni has a little concentric ring core–shell nanostructure (Fig. 2b) after calcination of the Ni solid sphere (Fig. 2a). NiO/Ni–N-CDs0.05 not only possesses concentric ring core–shell nanostructures, but also exhibits an expanded shell layer, a diminished core, and an opening on the shell layer's surface (Fig. 2c). The HRTEM image of NiO/Ni–N-CDs0.05 exhibits well-resolved lattice fringes with interplanar spacings of 0.203 and 0.208 nm, which corresponds to the (111) crystal plane of Ni and the (200) crystal plane of NiO, respectively.[38,39] The interplanar spacings of 0.260 and 0.321 nm belong to N-CDs, which indicates that the N-CDs were successfully introduced into NiO/Ni.[40] The TEM image (Fig. 2e) and the high-angle annular dark-field (HAADF) images show the elemental distribution of Ni, O and C (Fig. 2f), and further show that the synthesized NiO/Ni–N-CDs0.05 has the structure of concentric rings.

X-ray photoelectron spectroscopy (XPS) was employed to reveal the chemical states and coordination environment of

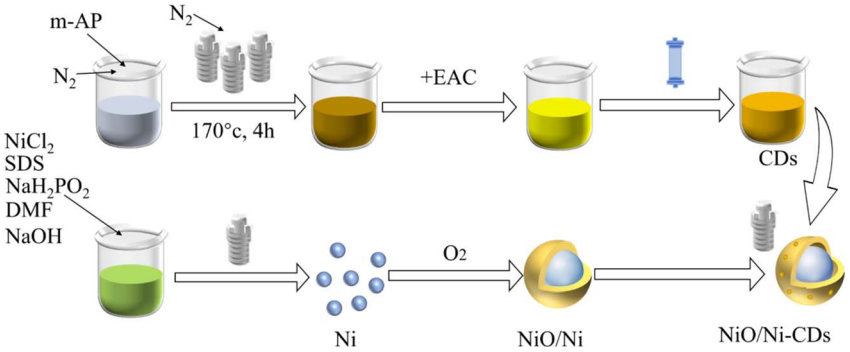

Scheme 1 Schematic illustration of the evolution of the structure of as-synthesized samples.

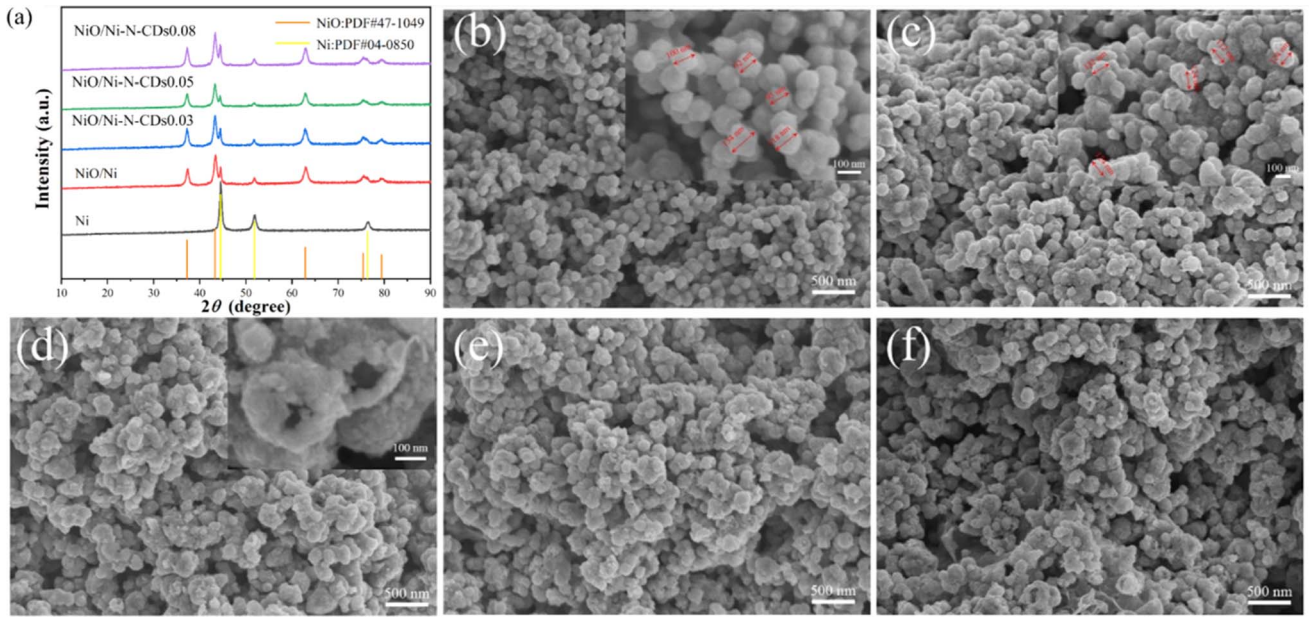

Fig. 1 PXRD patterns (a) and SEM images of Ni (b), NiO/Ni (c), NiO/Ni–N-CDs0.03 (d), NiO/Ni–N-CDs0.05 (e) and NiO/Ni–N-CDs0.08 (f).

atoms on the surface of the as-synthesized material to verify the effect of the addition of carbon dots on the samples. The detailed data obtained during XPS peak fitting are provided in Table S1.† The survey spectra of XPS are shown in Fig. 3a, and the elements of Ni, O and C are present in both NiO/Ni and NiO/Ni–N-CDs0.05. The high-resolution XPS (HR-XPS) spectra of C 1s are presented in Fig. 3b; three peaks centered at 284.8, 286.2 and 288.4 eV are attributed to C–C, C–OH, and C=O, respectively.[41] As shown in Fig. 3c, the Ni 2p displays two binding energy peaks at 853.2 and 871.1 eV, indicating the presence of Ni^0 in the as-synthesized samples.[42] In addition, the two peaks located at 855.5 and 873.1 eV are ascribed to Ni $2p_{3/2}$ and Ni $2p_{1/2}$ of Ni^{II}.[43] The other two peaks at 861.1 and 879.6 eV are attributed to the satellite's peak.[44] The ratio of NiO/Ni was obtained from the XPS spectra, and the results were to be 75.4% and 77.1% in the NiO/Ni and NiO/Ni–N-CDs0.05, respectively. The O 1s spectra in Fig. 3d display three peaks at 529.3, 531.1 and 533.2 eV, respectively, assigned to the O–Ni, C–O, and O–C–O.[45] The positions of fitting peaks for all elements are almost unchanged. Still, the content of C–OH and O–C–O increased significantly after the introduction of N-CDs, indicating that there were more active species on the surface of NiO/Ni–N-CDs0.05.

3.2 Electro-oxidation of methanol in the presence of NiO/Ni–N-CDs

The electrocatalytic methanol oxidation reaction was explored after determining the composition and structure of the as-synthesized samples. Fig. 4a displays the CV curves obtained in a 1 M KOH electrolyte at 50 mV s^{-1} and shows the low current density. When 1 M methanol was added to the KOH electrolyte, the current density increases obviously (Fig. 4b). The CV curves of N-CDs, Ni–N-CDs and NiO/Ni–N-CDs in a 1 M KOH electrolyte and after the addition of a 1 M methanol electrolyte are displayed in Fig. S5,† which suggests that the NiO/Ni–N-CDs have a larger current density than that of the

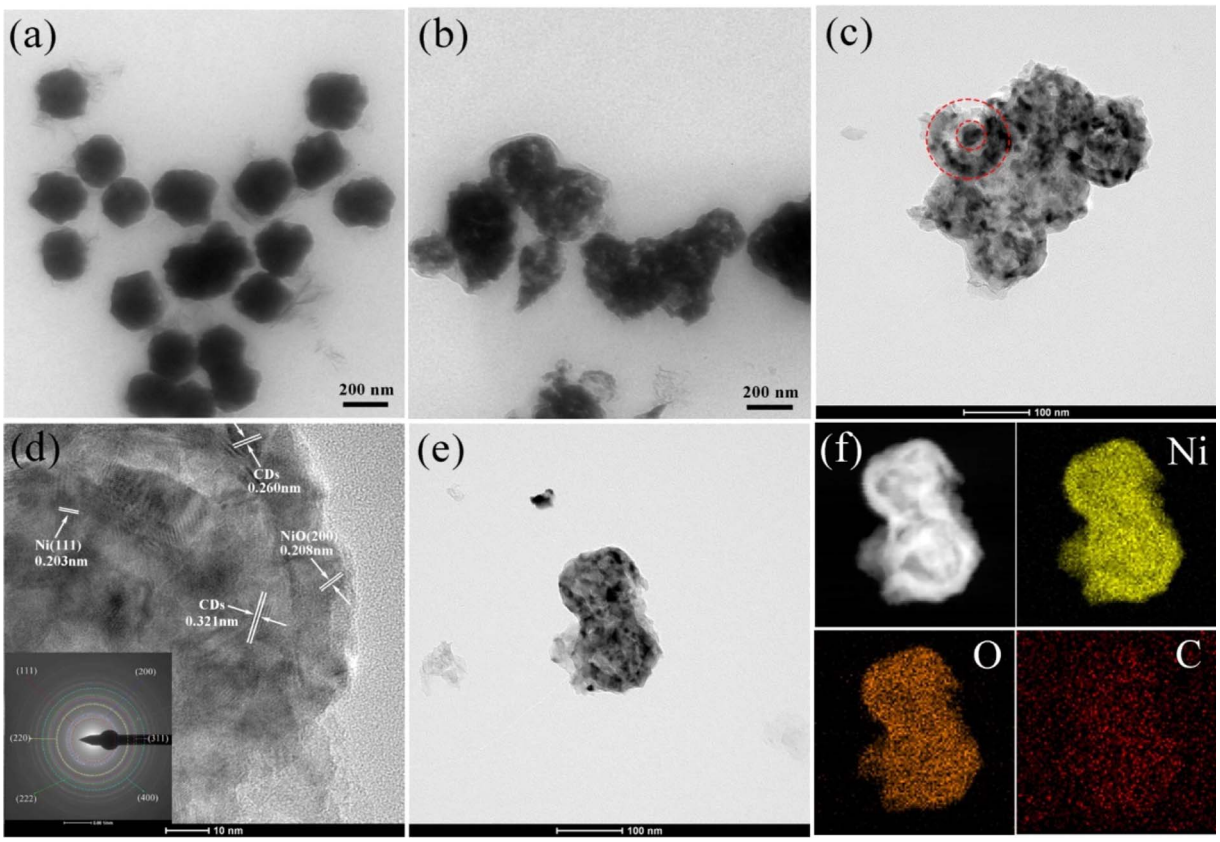

Fig. 2 TEM images of Ni (a), NiO/Ni (b) and NiO/Ni–N-CDs0.05 (c). HR-TEM image of NiO/Ni–N-CDs0.05 (d and e). EDX elemental mapping of NiO/Ni–N-CDs0.05 (f).

other samples. NiO/Ni–N-CDs0.05 possesses the optimal catalytic activity, and the current density reached 47.32 mA cm^{-2}, which is 3.02-fold than that of NiO/Ni (15.67 mA cm^{-2}). Meanwhile, the current density is increased by 93.95% compared to that in the KOH electrolyte. The mass activities of the as-synthesized samples are shown in Fig. 4c, and the catalytic activity was significantly improved with the addition of N-CDs. As depicted in Fig. 4d, the mass activities are in the order of NiO/Ni–N-CDs0.05 (228.2 ± 16.6 A g^{-1}) > NiO/Ni–N-CDs0.03 (133.7 ± 14.3 A g^{-1}) > NiO/Ni–N-CDs0.08 (97.5 ± 7.4 A g^{-1}) > NiO/Ni (68.8 ± 1.1 A g^{-1}). The catalytic activity becomes superior after the introduction of N-CDs. These experiments were repeated three times and the data are presented as mean and standard deviations (error bar). However, with the increase in the content of N-CDs, the catalytic activity first increases and then decreases, which is in good agreement with the trend of structural change.

Moreover, the electrochemically active surface area (ECSA) of the as-synthesized samples is one of the important parameters used to measure the MOR activity. The ECSA was obtained by measuring the double-layer capacitance (C_{dl}) from the CV curves with different scan rates (Fig. S6†).[46] The C_{dl} value was calculated by the corresponding linear fit of the capacitive current *vs.* scan rates, according to formula (S2) (Fig. S7).†[47] The value of ECSA was recorded in Fig. 4e, and the ECSA value of NiO/Ni–N-CDs0.05 was estimated to be 69.5 m^2 g^{-1}, which is noticeably larger than those of NiO/Ni (28.5 m^2 g^{-1}), NiO/Ni–N-CDs0.03 (48.3 m^2 g^{-1}) and NiO/Ni–N-CDs0.08 (32.2 m^2 g^{-1}). The significant increment of ECSA for NiO/Ni–N-CDs0.05 can be attributed to the structure of concentric rings, good electrical conductivity, accessible interior/exterior surface, and abundant active sites. Electrochemical impedance spectroscopy (EIS) was carried out to explain the enhanced catalytic activity.[48] As shown in Fig. 4f, NiO/Ni–N-CDs0.05 exhibits the smallest radius, confirming the lowest charge transfer resistance (R_{ct}) and the fastest interfacial charge transfer process.[49] The stability was studied by chronoamperometry to assess the practical application potential of the sample in the field of methanol oxidation.[50] Fig. S8† shows the chronoamperometry curves for all the samples during the MOR. The NiO/Ni–N-CDs0.05 shows good stability throughout the entire period, where no significant change is observed throughout the 83 h. The SEM images (Fig. S9†) and XRD patterns (Fig. S10†) of NiO/Ni–N-CDs0.05 after stability tests confirm the structural stability during the MOR. Fig. S11† depicts the XPS spectra of NiO/Ni–N-CDs after the stability test. The C 1s spectrum is shown in Fig. S11a.† The binding energy of Ni 2p shows a slight positive shift (Fig. S11b†), indicating that Ni is the main active site during the MOR process.[51] Fig. S11c† shows the O 1s spectra, where the Ni–O bonding has

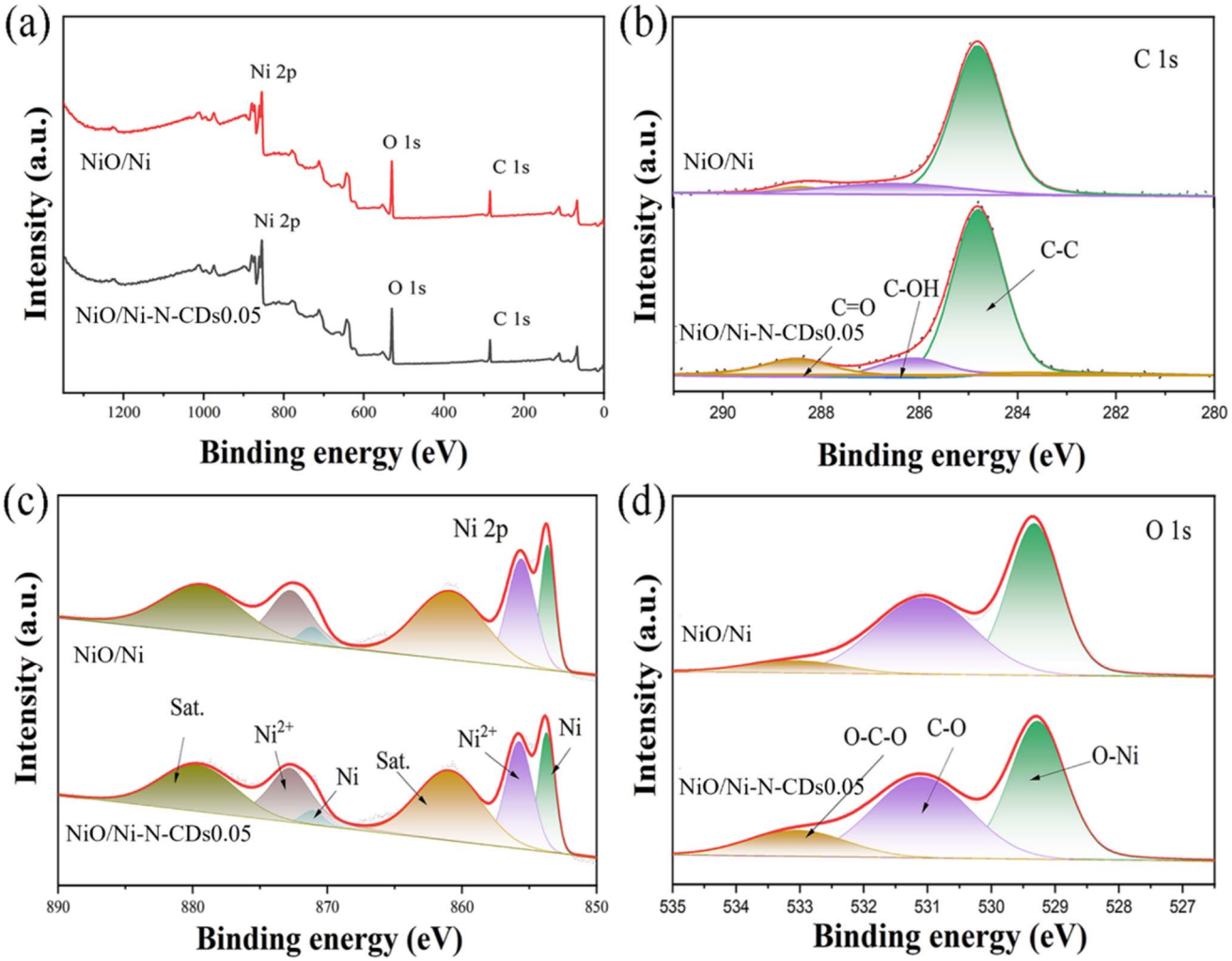

Fig. 3 XPS spectra survey (a), HR-XPS spectra of C 1s (b), Ni 2p (c) and O 1s (d) of NiO/Ni and NiO/Ni–N-CDs0.05.

almost disappeared compared to the pristine one, and H_2O appears at a peak of 532.1 eV. The increased O–C–O bonding may be due to the incorporation of carbon black during the sample preparation process.[52]

Apart from the MOR, the oxidation properties of other alcohols have also been investigated. As shown in Fig. 5, the oxidation reaction of ethanol (EOR), ethylene glycol (EGOR) and glycerol (GOR) were examined on the as-synthesized samples. Fig. 5a–c display the significantly enhanced current density after the introduction of N-CDs, and the NiO/Ni–N-CDs0.05 possesses optimal performance whether at EOR, EGOR or GOR. The mass activity of NiO/Ni–N-CDs0.05 reached 405.9 $\pm$ 27.3 A g^{-1}, 169.90 $\pm$ 3.4 A g^{-1} and 141.6 $\pm$ 9.7 A g^{-1} for EOR, EGOR and GOR, respectively (Fig. 5d–f). These results further verify the extremely high oxidation activity of NiO/Ni–N-CDs0.05 for alcohols after the introduction of appropriate N-CDs. These tests were repeated three times and the data were expressed as mean and standard deviation (error bars). Compared with other non-Pt-based catalysts, NiO/Ni–N-CDs 0.05 exhibits a good electrocatalytic performance (Table 1).

The superior electrocatalytic activity of precisely designed NiO/Ni–N-CDs0.05 may be due to the unique structural advantages and the synergistic effect of N-CDs. The structure of concentric rings with an opening shell provided an accessible interior/exterior surface and highly exposed active sites for the adsorption of methanol. There were abundant active species on the surface of the material after the introduction of N-CDs, which is conducive to the intermediate process of MOR.[60–62] The samples containing N-CDs have enlarged Brunauer–Emmett–Teller (BET) specific surface areas (Fig. S12†). Moreover, ECSA was positively correlated with the oxidation rate, and NiO/Ni–N-CDs0.05 possesses a large ECSA value.[63] This indicates that there is a rapid oxidation reaction occurring on the NiO/Ni–N-CDs0.05 surface. Meanwhile, the presence of N-CDs reduces the electrochemical impedance and improves the electrochemical conductivity.[64] Hence, NiO/Ni–N-CDs0.05 acts as a non-noble metal effective electrocatalyst for alcohol oxidation reaction with the unique structure of concentric rings and the advantages of N-CDs.

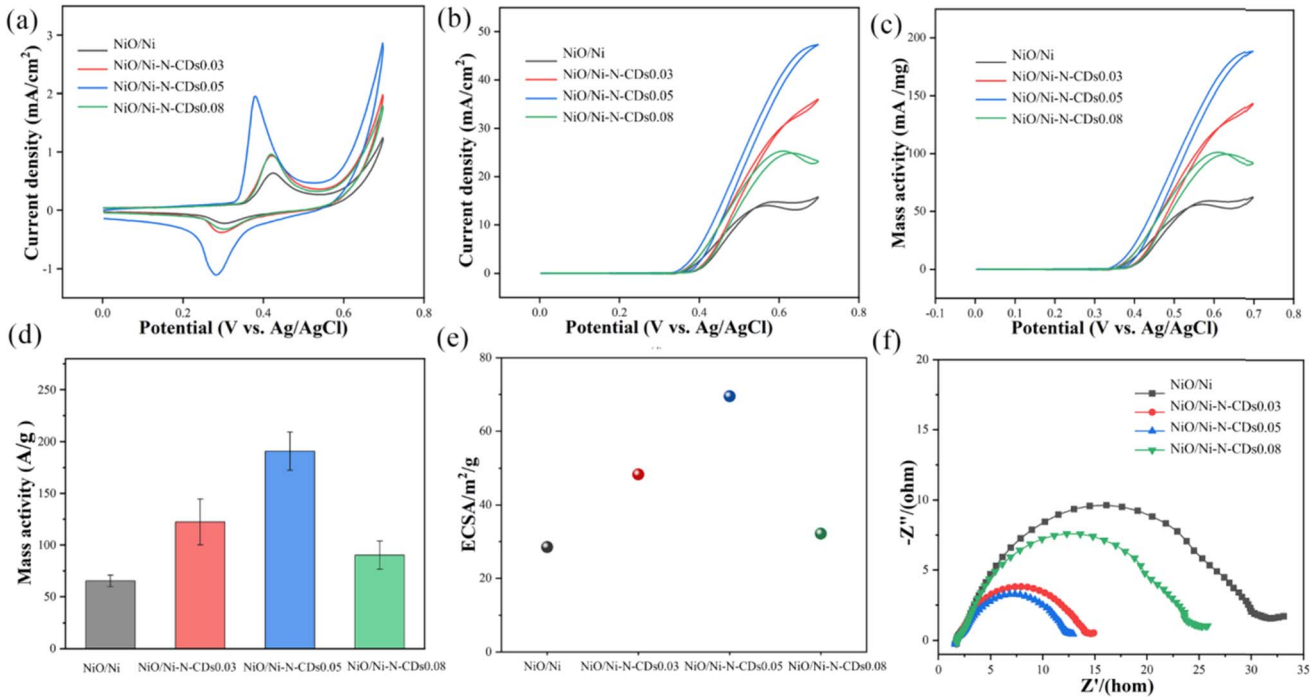

Fig. 4 Electrocatalytic performance of the as-synthesized samples for MOR. CV curves of NiO/Ni, NiO/Ni–N-CDs0.03, NiO/Ni–N-CDs0.05 and NiO/Ni–N-CDs0.08 in (a) 1 M KOH and (b) 1 M KOH + 1 M CH_3OH. (c and d) Mass activity, (e) ECSAs and (f) EIS Nyquist plots of different samples.

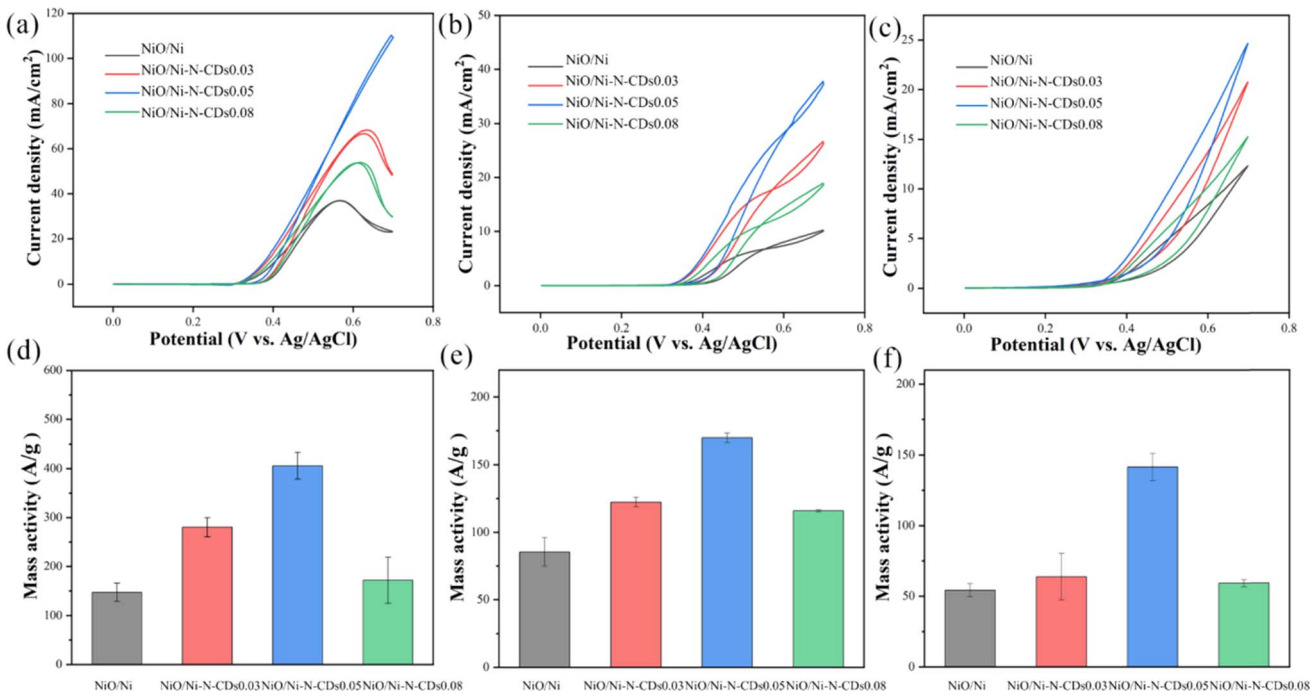

Fig. 5 CV curves of NiO/Ni, NiO/Ni–N-CDs0.03, NiO/Ni–N-CDs0.05 and NiO/Ni–N-CDs0.08 in (a) 1 M ethanol + 1 M KOH, (b) 1 M ethylene glycol + 1 M KOH and (c) 1 M glycerol + 1 M KOH. Mass activity of NiO/Ni, NiO/Ni–N-CDs0.03, NiO/Ni–N-CDs0.05 and NiO/Ni–N-CDs0.08 in (d) 1 M ethanol + 1 M KOH, (e) 1 M ethylene glycol + 1 M KOH and (f) 1 M glycerol + 1 M KOH.

Table 1 Comparison of the MOR performance of NiO/Ni–N-CDs0.05 with that of the recently reported electrocatalysts

Catalysts	Electrolytes	Scan rate ($mV\ s^{-1}$)	Current density ($mA\ cm^{-2}$)	Reference
NiO/Ni–N-CDs0.05	1 M KOH + 1 M CH_3OH	50	47.32	This work
CNFs-Ni	1 M KOH + 0.5 M CH_3OH	50	1.7	53
PtCo CNCs	0.5 M H_2SO_4 + 1.0 M CH_3OH	50	3.04	54
PtPd HNCs-E	0.1 M KOH + 1 M CH_3OH	50	6.7	55
Ni/CN	1 M NaOH + 1 M CH_3OH	50	~6.3	56
3D Ni/NiO/RG-400	1 M KOH + 1 M CH_3OH	50	79.50	57
Cu/NiCu NWs/C	1 M KOH + 1 M CH_3OH	50	34.9	58
Poly[Ni(salen)]ATV	1 M KOH + 0.1 M CH_3OH	50	14.1	59

4. Conclusions

In summary, we reported non-noble metal NiO/Ni-based materials with incorporated carbon dots as model electrocatalysts for methanol electro-oxidation reactions. The unique concentric ring structures with accessible interior/exterior surfaces significantly enhanced the electrochemical reactivity for the MOR after the introduction of carbon dots. The optimal catalyst, denoted as NiO/Ni–N-CDs0.05, achieved a current density that is 3.02 times higher than that of the pristine NiO/Ni in a solution of 1 M KOH + 1 M CH_3OH. However, an excess of carbon dots can lead to a decrease in current density due to the blocking of active sites. The NiO/Ni–N-CDs0.05 material exhibited superior electrochemical conductivity to NiO/Ni. Furthermore, the electrocatalytic activities of various alcohols such as ethanol, ethylene glycol, and glycerol were also investigated, showing the versatility of the catalyst. This work provides a promising strategy for improving the electrocatalytic activity by constructing a unique concentric ring structure and by effectively utilizing the synergistic effects of non-noble metal catalysts and carbon dots. This approach offers a cost-effective and efficient pathway for the development of high-performance electrocatalysts for direct methanol fuel cell applications.

Data availability

The data supporting this article have been included as part of the ESI.†

Conflicts of interest

The authors declare that they have no known competing financial interests or personal relationships that could have appeared to influence the work reported in this paper.

Acknowledgements

We gratefully acknowledge the Natural Science Foundation of Anhui Higher Education Institutions of China (No. 2023AH051761, KJ2021A0825), the Key Research Culture Funds of Wannan Medical College (No. WK2022Z02), National Innovation and Entrepreneurship Training for University of PRC (202310368045, S202310368080, S202210368124), the Excellent Young Talents Fund Program of Higher Education Institutions of Anhui Province (gxyq2022046), State Key Laboratory of Coordination Chemistry of Nanjing University (No. SKLCC2414) for financial support of this work.

References

1 A. Yadav, Y. Li, T.-W. Liao, K.-J. Hu, J. E. Scheerder, O. V. Safonova, T. Höltzl, E. Janssens, D. Grandjean and P. Lievens, Enhanced methanol electro-oxidation activity of nanoclustered gold, *Small*, 2021, **17**, 2004541, DOI: 10.1002/smll.202004541.

2 L. Huang, X. Zhang, Q. Wang, Y. Han, Y. Fang and S. Dong, Shape-control of pt-ru nanocrystals: tuning surface structure for enhanced electrocatalytic methanol oxidation, *J. Am. Chem. Soc.*, 2018, **140**, 1142–1147, DOI: 10.1021/jacs.7b12353.

3 N. Metzger and X. Li, Technical and economic analysis of fuel cells for forklift applications, *ACS Omega*, 2022, **7**, 18267–18275, DOI: 10.1021/acsomega.1c07344.

4 R. E. Khalifa, A. M. Omer, M. H. Abd Elmageed and M. S. Mohy Eldin, Titanium dioxide/phosphorous-functionalized cellulose acetate nanocomposite membranes for DMFC applications: enhancing properties and performance, *ACS Omega*, 2021, **6**, 17194–17202, DOI: 10.1021/acsomega.1c00568.

5 A. Yuda, A. Ashok and A. Kumar, A comprehensive and critical review on recent progress in anode catalyst for methanol oxidation reaction, *Catal. Rev.*, 2022, **64**, 126–228, DOI: 10.1080/01614940.2020.1802811.

6 Y. Li, E. Zhu, J. Yu, J. Yu, J. Yang, W. Liu, X. Cui, X. Yang, Y. Zhang and M. Xu, Pt-Ni nanoparticles electrodeposited on rGO/CFP as high-performance integrated electrode for methanol oxidation, *Int. J. Hydrogen Energy*, 2022, **47**, 23957–23970, DOI: 10.1016/j.ijhydene.2022.05.162.

7 R. Sarkar, A. A. Farghaly and I. U. Arachchige, Oxidative self-assembly of Au/Ag/Pt alloy nanoparticles into high-surface area, mesoporous, and conductive aerogels for methanol electro-oxidation, *Chem. Mater.*, 2022, **34**, 5874–5887, DOI: 10.1021/acs.chemmater.2c00717.

8 T. Shao, Q. Zhang, J. Li, S. He, D. Zhang and X. Zhou, AgPt hollow nanodendrites based on N doping graphene quantum dots for enhanced methanol electrooxidation, *J.*

Alloys Compd., 2021, **882**, 160607, DOI: 10.1016/j.jallcom.2021.160607.

9 G. Vishwakshan Reddy, Y. Chandra Sekhar, P. Raghavendra, M. Narendra Reddy, P. Sri Chandana and L. Subramanyam Sarma, Controlled synthesis of reduced graphene oxide-supported bimetallic Pt-Au nanoparticles for enhanced electrooxidation of methanol, *Solid State Sci.*, 2024, **149**, 107469, DOI: 10.1016/j.solidstatesciences.2024.107469.

10 H.-H. Li, Q.-Q. Fu, L. Xu, S.-Y. Ma, Y.-R. Zheng, X.-J. Liu and S.-H. Yu, Highly crystalline PtCu nanotubes with three dimensional molecular accessible and restructured surface for efficient catalysis, *Energy Environ. Sci.*, 2017, **10**, 1751–1756, DOI: 10.1039/C7EE00573C.

11 P. Yao, J. Cao, M. Ruan, P. Song, X. Gong, C. Han and W. Xu, Engineering PtCu nanoparticles for a highly efficient methanol electro-oxidation reaction, *Faraday Discuss.*, 2022, **233**, 232–243, DOI: 10.1039/D1FD00047K.

12 L. Bai, Synthesis of PtRu/Ru heterostructure for efficient methanol electrooxidation: The role of extra Ru, *Appl. Surf. Sci.*, 2018, **433**, 279–284, DOI: 10.1016/j.apsusc.2017.10.026.

13 Y. Shi, W. Zhu, H. Shi, F. Liao, Z. Fan and M. Shao, Mesocrystal PtRu supported on reduced graphene oxide as catalysts for methanol oxidation reaction, *J. Colloid Interface Sci.*, 2019, **557**, 729–736, DOI: 10.1016/j.jcis.2019.09.038.

14 J. Zhao, Y. Zhou, L. Qin and M. Zhao, Synthesis of Pt-Co micro/nanoporous array with high activity for methanol electrooxidation, *Mater. Lett.*, 2018, **216**, 166–169, DOI: 10.1016/j.matlet.2018.01.023.

15 W. Chen, J. Xue, Y. Bao and L. Feng, Surface engineering of nano-ceria facet dependent coupling effect on Pt nanocrystals for electro-catalysis of methanol oxidation reaction, *Chem. Eng. J.*, 2020, **381**, 122752, DOI: 10.1016/j.cej.2019.122752.

16 L. Zhuang, Z. Jia, Y. Wang, X. Zhang, S. Wang, J. Song, L. Tian and T. Qi, Nitrogen-doped carbon black supported synergistic palladium single atoms and nanoparticles for electrocatalytic oxidation of methanol, *Chem. Eng. J.*, 2022, **438**, 135585, DOI: 10.1016/j.cej.2022.135585.

17 T. N. Pham, A. Samikannu, S. Tesfalidet, T. Wagberg and J.-P. Mikkola, NiCo nanoneedles on 3D carbon nanotubes/carbon foam electrode as an efficient bi-functional catalyst for electro-oxidation of water and methanol, *Catalysts*, 2021, **11**, 500, DOI: 10.3390/catal11040500.

18 R. Huang, Y. Sun, X. Zhang, B. Sun, Q. Wang and J. Zhu, Biological evaluation of a novel Herceptin-platinum (II) conjugate for efficient and cancer cell specific delivery, *Biomed. Pharmacother.*, 2015, **73**, 116–122, DOI: 10.1016/j.biopha.2015.05.013.

19 Y. Wang, X.-M. Zhang, Y. Sun, H.-L. Chen and L.-Y. Zhou, Cetuximab-decorated and NIR-activated nanoparticles based on platinum(IV)-prodrug: preparation, characterization and in-vitro anticancer activity in epidermoid carcinoma cells, *Iran. J. Pharm. Res.*, 2021, **20**, 371–383, DOI: 10.22037/ijpr.2020.113439.14303.

20 S. Liu, Y.-Y. Sun, Y.-P. Wu, Y.-J. Wang, Q. Pi, S. Li, Y.-S. Li and D.-S. Li, Common Strategy: mounting the Rod-like Ni-Based MOF on Hydrangea-Shaped Nickel Hydroxide for Superior Electrocatalytic Methanol Oxidation Reaction, *ACS Appl. Mater. Interfaces*, 2021, **13**, 26472–26481, DOI: 10.1021/acsami.1c04282.

21 E. Saeed, I. Abdelwahab and A. Abdelwahab, Ni-Co-P functionalized Nitrogen-Doped-Carbon quantum dots for efficient methanol electrooxidation and nanofluid applications, *J. Electroanal. Chem.*, 2023, **928**, 117083, DOI: 10.1016/j.jelechem.2022.117083.

22 Y. Yang, H. Li, H. Xie and J. Q. Hao, Carrier-free, pure nanodrugs based on dasatinib and 5-Fluorouracil show aggregation-induced emission and enhanced antitumor efficacy, *J. Drug Delivery Sci. Technol.*, 2023, **90**, 105142, DOI: 10.1016/j.jddst.2023.105142.

23 E. A. Şahin and R. Solmaz, Methanol electrooxidation activity of binary CoAg electrocatalyst, *Int. J. Hydrogen Energy*, 2020, **45**, 35013–35022, DOI: 10.1016/j.ijhydene.2020.08.125.

24 M. Abbas, R. M. Abdel Hameed, A. M. Al-Enizi, B. M. Thamer, A. Yousef and M. H. El-Newehy, Decorated carbon nanofibers with mixed nickel-manganese carbides for methanol electro-oxidation in alkaline solution, *Int. J. Hydrogen Energy*, 2021, **46**, 6494–6512, DOI: 10.1016/j.ijhydene.2020.11.153.

25 M. B. Askari, P. Salarizadeh, A. Di Bartolomeo, M. H. Ramezan zadeh, H. Beitollahi and S. Tajik, Hierarchical nanostructures of $MgCo_2O_4$ on reduced graphene oxide as a high-performance catalyst for methanol electro-oxidation, *Ceram. Int.*, 2021, **47**, 16079–16085, DOI: 10.1016/j.ceramint.2021.02.182.

26 Y. Sun, T. Shi, L. Zhou, Y. Zhou, B. Sun and X. Liu, Folate-decorated and NIR-activated nanoparticles based on platinum(IV) prodrugs for targeted therapy of ovarian cancer, *J. Microencapsulation*, 2017, **34**, 675–686, DOI: 10.1080/02652048.2017.1393114.

27 M. B. Askari, P. Salarizadeh, A. D. Bartolomeo and F. Şen, Enhanced electrochemical performance of $MnNi_2O_4$/rGO nanocomposite as pseudocapacitor electrode material and methanol electro-oxidation catalyst, *Nanotechnology*, 2021, **32**, 325707, DOI: 10.1088/1361-6528/abfded.

28 H. Hong, Q. Zou, Y. Liu, S. Wang, G. Shen and X. Yan, Supramolecular nanodrugs based on covalent assembly of therapeutic peptides toward in vitro synergistic anticancer therapy, *ChemMedChem*, 2021, **16**, 2381–2385, DOI: 10.1002/cmdc.202100236.

29 B. Yang, Y. Yu, J. Qiao, L. Yuan, X. Shen and X. Hu, Solution plasma method for the preparation of Cu-Ni/CuO-NiO with excellent methanol electrocatalytic oxidation performance, *Appl. Surf. Sci.*, 2020, **513**, 145808, DOI: 10.1016/j.apsusc.2020.145808.

30 Z. Liu, P. Chang, M. Xi, J. Ding, X. Wang, J. Wang, W. Zhang and Y. Huang, Synthesis of Ni_3B/Ni via vacuum-induced for ultrahigh stable and efficient methanol oxidation, *Small*, 2023, **19**, 2303855, DOI: 10.1002/smll.202303855.

31 F.-K. Chen, Y.-H. Ho, H.-W. Chang and Y.-C. Tsai, Nanocomposite integrating tube-like $NiCo_2S_4$ and carbon nanotubes for electrooxidation of methanol, *Electrochem.*

Commun., 2020, **117**, 106783, DOI: 10.1016/j.elecom.2020.106783.

32 P. Raghavendra, G. V. Reddy, R. Sivasubramanian, P. S. Chandana and L. S. Sarma, Facile Fabrication of Pt-Ru Nanoparticles Immobilized on Reduced Graphene Oxide Support for the Electrooxidation of Methanol and Ethanol, *ChemistrySelect*, 2017, **2**, 11762–11770, DOI: 10.1002/slct.201702636.

33 P. Das, M. Sherazee, P. K. Marvi, S. R. Ahmed, A. Gedanken, S. Srinivasan and A. R. Rajabzadeh, Waste-Derived Sustainable Fluorescent Nanocarbon-Coated Breathable Functional Fabric for Antioxidant and Antimicrobial Applications, *ACS Appl. Mater. Interfaces*, 2023, **15**, 29425–29439, DOI: 10.1021/acsami.3c03778.

34 P. Das, S. Ganguly, A. Saravanan, S. Margel, A. Gedanken, S. Srinivasan and A. R. Rajabzadeh, Naturally Derived Carbon Dots In Situ Confined Self-Healing and Breathable Hydrogel Monolith for Anomalous Diffusion-Driven Phytomedicine Release, *ACS Appl. Bio Mater.*, 2022, **5**, 5617–5633, DOI: 10.1021/acsabm.2c00664.

35 V. M. Naik, S. V. Bhosalec and G. B. Kolekar, A brief review on the synthesis, characterisation and analytical applications of nitrogen doped carbon dots, *Anal. Methods*, 2022, **14**, 877–891, DOI: 10.1039/D1AY02105B.

36 S. Wu, X. Wang, J. Bai, Y. Zhu, X. Yu, F. Qin, P. He and L. Ren, Influence of Nitrogen-Doped Carbon Quantum Dots on the Electrocatalytic Performance of the CoP Nanoflower Catalyst for OER, *Langmuir*, 2022, **38**, 11210–11218, DOI: 10.1016/j.colsurfa.2020.124758.

37 J. Huang, W. Chen, X. Yu, X. Fu, Y. Zhu and Y. Zhang, Fabrication of a ternary BiOCl/CQDs/rGO photocatalyst: The roles of CQDs and rGO in adsorption-photocatalytic removal of ciprofloxacin, *Colloids Surf., A*, 2020, **597**, 124758, DOI: 10.1016/j.colsurfa.2020.124758.

38 V. D. Silva, R. A. Raimundo, T. A. Simões, F. J. A. Loureiro, D. P. Fagg, M. A. Morales, D. A. Macedo and E. S. Medeiros, Nonwoven Ni-NiO/carbon fibers for electrochemical water oxidation, *Int. J. Hydrogen Energy*, 2021, **46**, 3798–3810, DOI: 10.1016/j.ijhydene.2020.10.156.

39 J. Wang, X. Ge, L. Shao, J. Zhang, D. Peng, G. Zou, H. Hou, W. Deng, S. Xu, X. Ji and W. Zhang, Reaction-driven transformation of Ni/NiO hybrid structure into Ni single atoms, *Mater. Today Energy*, 2020, **17**, 100436, DOI: 10.1016/j.mtener.2020.100436.

40 Y. Wei, L. Chen, J. Wang, X. Liu, Y. Yang and S. Yu, Investigation on the chirality mechanism of chiral carbon quantum dots derived from tryptophan, *RSC Adv.*, 2019, **9**, 3208–3214, DOI: 10.1039/C8RA09649J.

41 Y. Luo, W. Zhong, P. Huang, H. Ou, H. Fu, C. Liu, Z. Xiao and S. Xu, Improved electrocatalytic activity of Pt catalyst supported on core-shell CMs@NiO for methanol oxidation, *New J. Chem.*, 2021, **45**, 12879–12885, DOI: 10.1039/D1NJ01934A.

42 M. Chandran, A. Raveendran, A. Thomas, M. Vinoba, S. K. Jeong and M. Bhagiyalakshmi, Nickel decorated on platinum confined in MXene as an electrocatalyst for enhanced electrooxidation of methanol, *Synth. Met.*, 2023, **293**, 117260, DOI: 10.1016/j.synthmet.2022.117260.

43 X. Dao, M. Nie, H. Sun, W. Dong, Z. Xue, Q. Li, J. Liao, X. Wang, X. Zhao, D. Yang and L. Teng, Electrochemical performance of metal-organic framework MOF(Ni) doped graphene, *Int. J. Hydrogen Energy*, 2022, **47**, 16741–16749, DOI: 10.1016/j.ijhydene.2022.03.176.

44 Y. Zhang, C. Chen, Q.-H. Zheng, Z.-K. Guo, B.-X. Dong and Y.-L. Teng, S-Doped NiII-Triazolate derived Ni-S-C catalyst for electrochemical CO_2 reduction to CO, *ACS Appl. Energy Mater.*, 2023, **6**, 9065–9073, DOI: 10.1021/acsaem.2c02333.

45 Y. Sun, Z. Zhang, C. Xiang, Y. Jiang, Y. Feng, X. Cheng, X. Li and M. Wang, Novel stalactiform structural CoNi-rGO for supercapacitors with enhanced electrochemical performance, *CrystEngComm*, 2024, **26**, 1843–1851, DOI: 10.1039/d3ce01240a.

46 J. Li, Y. Zuo, J. Liu, X. Wang, X. Yu, R. Du, T. Zhang, M. F. Infante-Carrió, P. Tang, J. Arbiol, J. Llorca, Z. Luo and A. Cabot, Superior methanol electrooxidation performance of (110)-faceted nickel polyhedral nanocrystals, *J. Mater. Chem. A*, 2019, **7**, 22036–22043, DOI: 10.1039/C9TA07066D.

47 A. Karmakar and S. Kundu, A concise perspective on the effect of interpreting the double layer capacitance data over the intrinsic evaluation parameters in oxygen evolution reaction, *Mater. Today Energy*, 2023, **33**, 101259, DOI: 10.1016/j.mtener.2023.101259.

48 B. B. Jin, H. S. Huang, S. Y. Kong, G. Q. Zhang, B. Yang, C. X. Jiang, Y. Zhou, D. J. Wang and J. H. Zeng, Antimony tin oxide/lead selenide composite as efficient counter electrode material for quantum dot-sensitized solar cells, *J. Colloid Interface Sci.*, 2021, **598**, 492–499, DOI: 10.1016/j.jcis.2021.04.073.

49 Q. Ma, J. Young, S. Basuray, G. Cheng, J. Gao, N. Yao and W. Zhang, Elucidating facet dependent electronic and electrochemical properties of CuO nanocrystals using AFM/SCEM and DFT_2, *Nano Today*, 2022, **45**, 101538, DOI: 10.1016/j.nantod.2022.101538.

50 M. Sadek, H. M. Abd El-Lateef, H. S. Mohran and M. Elrouby, A promising star-like PtNi and coral reefs-like PtCo nano-structured materials for direct methanol fuel cell application, *Electrochim. Acta*, 2021, **399**, 139370, DOI: 10.1016/j.electacta.2021.139370.

51 H. Su, W. Zhou, W. Zhou, Y. Li, L. Zheng, H. Zhang, M. Liu, X. Zhang, X. Sun, Y. Xu, F. Hu, J. Zhang, T. Hu, Q. Liu and S. Wei, In-situ spectroscopic observation of dynamic-coupling oxygen on atomically dispersed iridium electrocatalyst for acidic water oxidation, *Nat. Commun.*, 2021, **12**, 6118, DOI: 10.1038/s41467-021-26416-3.

52 J. Lin, J. Chen, C. Tan, Y. Zhang and Y. Li, Ruthenium-doped $Ni(OH)_2$ to enhance the activity of methanol oxidation reaction and promote the efficiency of hydrogen production, *RSC Adv.*, 2024, **14**, 18695–18702, DOI: 10.1039/D4RA02181A.

53 J. Wang, Q. Zhao, H. Hou, Y. Wu, W. Yu, X. Ji and L. Shao, Nickel nanoparticles supported on nitrogen-doped honeycomb-like carbon frameworks for effective methanol

oxidation, *RSC Adv.*, 2017, **7**, 14152–14158, DOI: **10.1039/C7RA00590C**.

54 Z. Li, X. Jiang, X. Wang, J. Hu, Y. Liu, G. Fu and Y. Tang, Concave PtCo nanocrosses for methanol oxidation reaction, *Appl. Catal.*, 2020, **277**, 119135, DOI: **10.1016/j.apcatb.2020.119135**.

55 Y.-X. Xiao, J. Ying, G. Tian, X.-Q. Zhang, C. Janiak, K. I. Ozoemena and X.-Y. Yang, PtPd hollow nanocubes with enhanced alloy effect and active facets for efficient methanol oxidation reaction, *Chem. Commun.*, 2021, **57**, 986–989, DOI: **10.1039/D0CC06876D**.

56 I. S. Pieta, A. Rathi, P. Pieta, R. Nowakowski, M. Hołdynski, M. Pisarek, A. Kaminska, M. B. Gawande and R. Zboril, Electrocatalytic methanol oxidation over Cu, Ni and bimetallic Cu–Ni nanoparticles supported on graphitic carbon nitride, *Appl. Catal., B*, 2019, **244**, 272–283, DOI: **10.1016/j.apcatb.2018.10.072**.

57 K. Zhang, Y. Han, J. Qiu, X. Ding, Y. Deng, Y. Wu, G. Zhang and L. Yan, Interface engineering of Ni/NiO heterostructures with abundant catalytic active sites for enhanced methanol oxidation electrocatalysis, *J. Colloid Interface Sci.*, 2023, **630**, 570–579, DOI: **10.1016/j.jcis.2022.10.057**.

58 D. Wu, W. Zhang and D. Cheng, Facile synthesis of Cu/NiCu electrocatalysts integrating alloy, Core–Shell, and one-dimensional structures for efficient methanol oxidation reaction, *ACS Appl. Mater. Interfaces*, 2017, **9**, 19843–19851, DOI: **10.1021/acsami.7b03876**.

59 J. L. Bott-Neto, T. S. Martins, S. A. S. Machado and E. A. Ticianelli, Electrocatalytic oxidation of methanol, ethanol, and glycerol on $Ni(OH)_2$ nanoparticles encapsulated with Poly[Ni(salen)] Film, *ACS Appl. Mater. Interfaces*, 2019, **11**, 30810–30818, DOI: **10.1021/acsami.9b08441**.

60 H. Javan, E. Asghari and H. Ashassi-Sorkhabi, Design of new anodic bimetallic nanocatalyst composed of Ni–Cu supported by reduced carbon quantum dots for the methanol oxidation reaction, *Diamond Relat. Mater.*, 2021, **115**, 108348, DOI: **10.1016/j.diamond.2021.108348**.

61 H. Javan, E. Asghari, H. Ashassi-Sorkhabi and M. Moradi-Haghighi, Nickel nanoparticles decorated on carbon quantum dots as a novel non-platinum catalyst for methanol oxidation; a green, low-cost, electrochemically-synthesized electrocatalyst, *Chem. Eng. Sci.*, 2020, **217**, 115534, DOI: **10.1016/j.ces.2020.115534**.

62 C. Luo, J. Yang, J. Li, S. He, B. Meng, T. Shao, Q. Zhang, D. Zhang and X. Zhou, Green synthesis of Au@N-CQDs@Pd core-shell nanoparticles for enhanced methanol electrooxidation, *J. Electroanal.*, 2020, **873**, 114423, DOI: **10.1016/j.jelechem.2020.114423**.

63 M. Abdullah, P. John, S. Manzoor, M. I. Ghouri, H. H. Hegazy, A. H. Chugtai, S. Aman, A. M. Shawky, M. N. Ashiq and T. A. Taha, Facile fabrication of CuO/AgSe nanosized composite via hydrothermal approach for the electrochemical energy conversion system2, *J. Energy Storage*, 2022, **56**, 105929, DOI: **10.1016/j.est.2022.105929**.

64 D. Pan, X. Li and A. Zhang, Platinum assisted by carbon quantum dots for methanol electro-oxidation, *Appl. Surf. Sci.*, 2018, **427**, 715–723, DOI: **10.1016/j.apsusc.2017.09.060**.